Journal of Applied Fluid Mechanics, Vol. 16, No. 2, pp. 223-231, 2023.
Available online at www.jafmonline.net, ISSN 1735-3572, EISSN 1735-3645.
https://doi.org/10.47176/jafm.16.02.1259

Experimental Study on Overall Cooling Effectiveness of Turbine Nozzle Guide Vane with Impingement-Cutback Structure

H. B. He, F. F. Duan and G. C. Li†

Shenyang Aerospace University, Shenyang 110000, China

†*Corresponding Author Email: ligc706@163.com*

(Received April 23, 2022; accepted September 20, 2022)

ABSTRACT

The overall cooling performance of turbine nozzle guide vane, with the impingement-cutback structure, is experimentally studied in the actual-scale cascade. The gas with the high temperature is used to achieve the actual dynamic viscosity coefficient and the density ratios. The coolant-to-gas mass flow ratio (K_G) varies between 0.034 and 0.050 and the gas-to-coolant temperature ratio (K_T) varies between 1.5 and 2.4. The local Overall Cooling Effectiveness (OCE) on the middle cross-section of the vane is obtained. The experimental results reveal that the lowest value of the OCE achieves a 10% relative arc length on the suction side of the vane; however, the highest value appears at 40% relative arc length on the pressure side of the vane. The averaged values of the OCE are respectively enhanced by 19.45%, 24.22%, and 35.57% at temperature ratios equal to 1.7, 1.9, and 2.3, with an increase of the K_G from 0.034 to 0.050. Added to that, it was identified that an increase of K_T from 1.7 to 2.3 leads to the decrease of the OCE. The comparison results show that this characteristic becomes dramatical while K_G is 0.034. The higher K_T leads to a greater influence of K_G, which is illustrated clearly by the compared results of the OCE.

Keywords: Turbine cooling; High temperature; Mass flow ratio; Temperature ratio; Impingement cooling.

NOMENCLATURE

avg	averaged
d	outer wall thickness of vane
c	coolant
G_C	mass flow rate of the coolant
G_g	mass flow rate through a passage of cascade
g	main stream
h_c	convective heat transfer coefficient
l	chord length of the middle cross profile of the vane
Nu	Nusselt number
P_g^*	total pressure at cascade inlet
Re	Reynolds number
S	arc length from the leading edge to the trailing edge in the middle cross profile of the vane
X	arc length coordinate starting from the stagnation point
T	temperature
u	velocity magnitude at vane cascade outlet
w	wall surface
θ	overall cooling effectiveness
λ	thermal conductivity
μ	dynamic viscosity coefficient
ρ	density

1. INTRODUCTION

Increasing turbine inlet temperature can lift the thrust of an aero-engine (Boyce 2011). However, the increased gas temperature leads to a strong thermal load on the turbine nozzle guide vane. The improvement of the vane material cannot meet the demand on the increase of the gas temperature. It must be relied on the effective cooling technology to guarantee the saft working of the turbine component. The cooling performance experiment in wind tunnel plays a crucial role in the designing a cooling structure process.

Many efforts have been made to explore the vane heat transfer issue through foundation model experiment. Huang *et al*. (1998) presented the influence of the outflow orientations on the

impinging jet orifice plate. The results showed that, when the entrance orientation was aligned with the exit flow, the peak value of the span averaged Nusselt number was significantly reduced. In addition, Han *et al*. (1991) found that the effect of the surface heat flux on the ribbed wall was much more significant in a square-form channel. Lots of studies have been published treating the influences of the blowing ratio, the length-diameter ratio, and the turbulence intensity on the film cooling effectiveness (Ekkad and Han 2015; Schroeder and Thole 2017; Andrews *et al*. 1989).

The evaluation of the overall cooling performance mainly relied on the external film cooling and the internal impingement cooling. An experimental research on the film cooling effectiveness of the cylindric holes, embedded in the saw-tooth slot, was conducted by Li *et al.* (2019). The influence of the slot depth on the film cooling effectiveness has shown opposite trend between low and high blowing ratios. Furthermore, the corner angle of saw tooth slot equal to 60° had a significantly high film effectiveness.

Moreover, the effect of hole structures on the film cooling effectiveness was analyzed by Sun *et al.* (2018) at the same mass flow rate of the coolant and the same region of the hole outlet. The researchers concluded that, for the film cooling effectiveness, the fan-shaped hole, the double jet holes and the sister holes presented the advanced performance, which were enhanced significantly compared to the cylindrical hole.

Both the film cooling effectiveness and heat transfer coefficient of four different cutback geometries were experimentally developed by Murata *et al.* (2012). Experiments show that the dimple surface was designed as an advanced cutback structure, since the heat transfer coefficient of it was increased without reducing the film cooling effectiveness.

Double-wall cooling was considered as an advanced technique for the innovation of the combustion chambers and turbine nozzle guide vanes for advanced aero-engines. Impingement cooling was applied in double-wall cooling technology (Han *et al.* 2012). The axial velocity of the jet is greatly affected by changing the outlet radius of the nozzle (Moussa *et al.* 2005). The impact of tangential the jet impinging on the heat transfer on the internal curved surfaces of the leading edge was also explored (Liu *et al.* 2018b). The tangential jet led to a significant increase in the heat transfer coefficient on the test surface. The heat transfer of the half-rough surfaces was found to be much more effective than that of traditional fully roughened surfaces (Lo and Liu 2018).

Furthermore, Lee *et al.* (2015) investigated the influences of the hole spacing between the separated and combined forms. In addition, the distance of the jet to target plate and the impact of Reynolds number on the heat transfer of the jet impingement was described precisely. The authors observed that the effectiveness of a single jet was reduced by the cross-flows accumulations from the continuous jet row. In addition, Fechter *et al*. (2013) conducted studies on heat transfer characteristics in narrow channels aiming to start the impingement cooling. They found out that the discharge coefficient was increased while enlarging the distance from the jet-to-target plate. The effect of the crossflow became more obvious with the shortened distance between the jet and the target plate. Andrew *et al*. (2010) proposed the impingement holes with elongated circular or elliptical shapes to increase the penetration of the jet impact through the coolant channel. It was shown that Nusselt numbers was increased from 28% to 77% under the first four impingement holes. This design can remarkably reduce the stress concentration factor, which is caused by the function of the holes.

Qu *et al*. (2017) explored the Overall Cooling Effectiveness (OCE) on the geometry using an integrated slot injection/effusion arrangement type. As described above, the integrated cooling pattern overcame the way of the single drawback caused by the decayed step and effused array cooling during the whole developing stage. In addition, Bryant *et al*. (2019) showed the influence of changing cooling structure on OCE through matched Biot number experiments. Facchini *et al.* (2010) proposed to increase the blowing ratio causing the weakened adiabatic effectiveness, thus enhancing the OCE of a series of effusion cooling for the end wall of the turbine. Furthermore, Yang *et al*. (2019) studied the coupling effect of Reynolds number and K_G on the endwall from the coolant to the mainstream. Aiming to explore the OCE of a blade endwall, both the jet impingement and the film cooling were carried out by Mensch and Karen (2014). They found clearly that, while the film cooling operated alone, the cooling efficiency was absolutely large around the holes caused by the convection cooling. The uniform cooling performance was attributed to the internal impingement, which seemed better than the film cooling. Mensch and Karen (2016) mentioned that the impingement cooling property was reduced due to the endwall contouring due to the enlargement of the role of the film cooling.

Rhee *et al*. (2017) obtained the OCE of the optimized arrangements of the hole through the experiments at various cooling mass flow rates. Many experiments have studied the OCE in low temperatures and low pressures condition. Due to the effect of the temperature on physical properties, the accuracy of the results will be inevitably affected while using the similarity criterion. Luque *et al*. (2016, 2017a, 2017b) used a new temperature parameter to define the OCE and expanded the hypothesis theory, which was verified by the experiments.

There are very few literatures resources regarding the OCE of impingement structures in high temperature condition. Thus, this experiment aims to present the distributions of the OCE of the vane with the impingement-cutback structure. The experi-mental conditions, including a total temperature of 1073 K and a total pressure of 0.55 MPa, were considered to be very close to the operating state of the turbine. Liu *et al*. (2018b) represented that to match engine operating conditions and laboratory conditions. In fact, K_T should be considered and matched with the

biot ratio at the mainstream side. The appropriate material is the key point to matching the biot ratio, which is ensured by using the practical blade during the experiments. When K_T is determined, the heat transfer coefficient ratio will also be confirmed. The temperature of 1073K gets close enough to match K_T. It means that both density ratio and dynamic viscosity coefficient ratio can be experimentally simulated in the meantime. Parametric tests with the operating factors, such as K_T and K_G, revealed the distributions of the OCE. The detailed heat transfer analysis provides a deeper understanding of the influences of K_G and K_T on the OCE.

Thus, this paper will be divided as follow: in section 2, the experimental apparatus and procedures will be presented whereas section 3 will show the results and the discussion. At the end, section 4 will conclude this work and propose some future ideas.

2. EXPERIMENTAL APPARATUS AND PROCEDURES

2.1 Experimental Apparatus

A schematic of the test system used for the vane cooling performance is shown in Fig. 1. The setup mainly consists of the air compressor, the combustion chamber and the actual-scale cascade with three vanes. The middle vane in the cascade is used to examine the cooling performance of the impingement-cutback structure. The inlet angle and outlet angle of the cascade are, respectively, 90° and 40°, and the geometry of the tested section is shown in Fig. 2. The applied air compressor has a maximum pressure capacity of 1.0 MPa, and the mass flow rate is as large as 2.4 kg/s. The mass flow rate of the mainstream is regulated by the inlet and the exhaust valves, and it is measured using the orifice flow meter. The coolant supply is implemented by the branched mainstream upstream of the inlet valve, and its mass flow rate is controlled by a separated regulating valve. The coolant air source is divided into two paths: one third of the coolant flows into the cavity of the test vane after heated by the electrical heater (the temperature and pressure measurement points are embedded at the inlet position of the cavity of the test vane) and the remaining two thirds of the coolant are used to afford the cooling application for the other two vanes. The pressure measuring point is fixed at the inlet of the cavity of the vane in order to have a similar pressure to that of the test vane. The coolant mass flow rate can be measured by the eddy current meter, with a maximal value of 0.06 kg/s.

As shown in Fig. 3, the test section is designed with a cooling layer having a circular shape where water is being driven by the pump to prevent the wall of the mainstream channel from being overheated and destroyed. The measuring points of the total temperature and the total pressure, in the cascade inlet, are respectively arranged at1.5 and 2 times of the chord length from the upstream of the leading edge of the vane. The five K-type thermocouples of the total temperature measuring point are located at 1/6, 1/3, 1/2, 2/3 and 5/6 to the corresponding height of vane respectively. One static pressure tap, inserted at one chord length downstream of the trailing edge, is used for monitoring the static pressure of the outlet of the cascade. The tested vanes have the same characteristic scale and material property as those installed on the engine to match the Biot number. A row of internal impingement holes is arranged at the leading edge of the vane. The impingement holes array with 3×8 and 4×20 are arranged at the pressure surface and the suction side. To measure the outer wall temperature, a total of 25 thermocouples are embedded on the middle cross profile of the vane as shown in Fig. 4.

2.2 Experimental Procedure

During the test, the mass flow rate of the mainstream is firstly adjusted by the inlet valve and the exhaust valve to meet the requirement for ignition. Then, the oil supply and the valve opening are gradually adjusted to meet the outlet Reynolds number of the cascade and the pressure ratio. The thermocouples measuring the temperature of the gas must be operating in the condition of non-cooling, so the temperature of the gas is controlled at 1073 K which is believed to be safe to the thermocouples. This temperature means that both the density ratio and the dynamic viscosity coefficient ratio can be experimentally simulated in the meantime. The required temperature, based on K_T, is obtained by the adjusted heater power. The data is recorded after the mass flow rate and temperature remain stable for two minutes. The Reynolds number of the cascade outlet is matched by changing the mainstream mass flow rate.

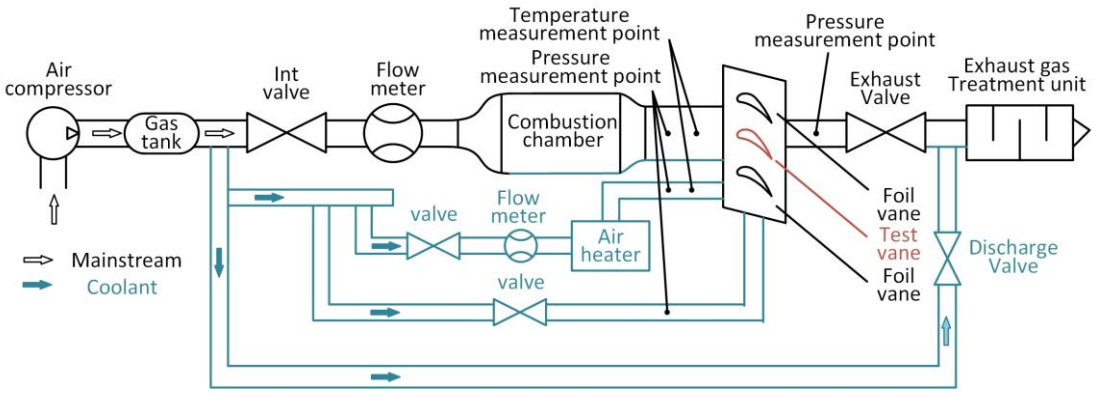

Fig. 1. Schematic of the vane cooling test system.

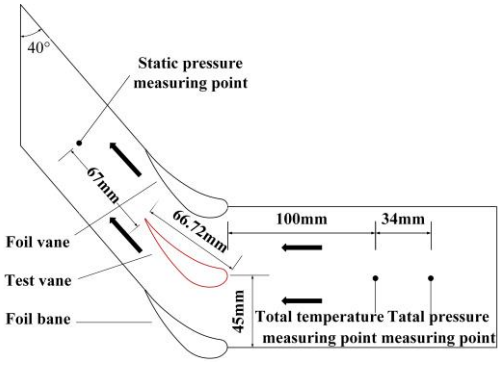

Fig. 2. Schematic of the turbine vane test section.

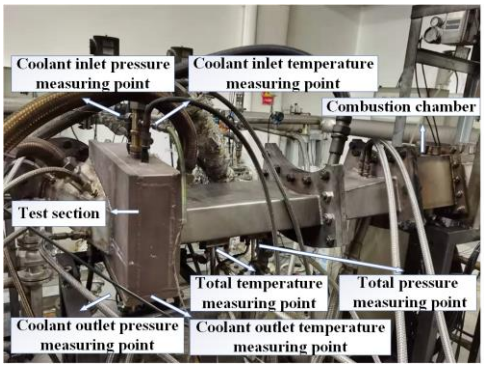

Fig. 3. Photograph of the test device.

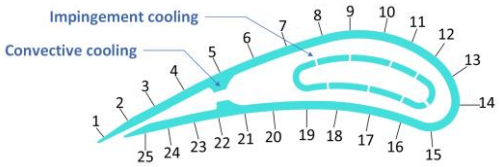

Fig. 4. schematic diagram of the test vane

All measurements were conducted in a steady state mode. Added to that, it was determined by monitoring the outputs of the thermocouples, the pressure sensors, and the flowmeters. Various values of K_T and K_G ranging from 1.5 to 2.4 and 0.034 to 0.050 were tested, respectively.

2.3 Parameter Definition and Working Conditions

The mass flow ratio is defined as:

$$K_G = \frac{G_C}{G_g} \quad , \tag{1}$$

where G_c is the mass flow rate of the coolant, and G_g is the mass flow rate of one single cascade passage.

The OCE is defined as follow:

$$\theta = \frac{(T_g^* - T_w)}{(T_g^* - T_c^*)} \quad , \tag{2}$$

where T_g^* is the total temperature of the gas, which is an averaged value of the five measured points of the temperature sensors, T_c^* is the temperature at the entrance of the coolant chamber and T_w is the surface temperature. The averaged value of the OCE is calculated by the temperatures measured by all of the thermocouples on the vane surface.

The temperature ratio is defined as:

$$K_T = \frac{T_g^*}{T_c^*} \quad . \tag{3}$$

The Reynolds number at the gas cascade outlet is defined as:

$$\mathrm{Re}_g = \frac{\rho_g u l}{\mu} \quad , \tag{4}$$

where l is the chord length at the middle cross profile of the turbine vane, u is the outlet gas velocity of the cascade, ρ_g is the density of the outlet gas, and μ is the dynamic viscosity coefficient.

The engine design point conditions are K_T = 1.9, and K_G = 0.042. The experimental parameters are selected according to the engine design parameters as shown in Table 1.

Table 1. Parameters in the experiment

Parameters	In experiment
K_G	0.034, 0.038, 0.042,0.046, 0.50
K_T	1.5, 1.7, 1.9, 2.1, 2.3
G_g [kg/s]	0.65
T_g^* [K]	1073
P_g^* [MPa]	0.55
Re_g	1.13×10^6

Table 2. Measurement instruments used in the experimental setup

Measurement instruments	Range
K-type thermocouple	273~1573[K]
Pressure transducer	0~1.6[MPa]

2.4 Uncertainty Analysis

The uncertainty of the OCE comes from the *K*-type thermocouple, whose uncertainty is 2 K. In light of the transfer formula, the uncertainty of the OCE is defined as follow:

$$d\theta = \sqrt{(\frac{\partial\theta}{\partial T_w})^2 dT_w^{\ 2} + (\frac{\partial\theta}{\partial T_g^*})^2 dT_g^{*2} + (\frac{\partial\theta}{\partial T_c^*})^2 dT_c^{*2}}$$

$$= \sqrt{\frac{(T_w - T_c^*)^2 dT_g^{*2}}{(T_g^* - T_c^*)^4} + \frac{(T_g^* - T_w)^2 dT_c^{*2}}{(T_g^* - T_c^*)^4} + \frac{dT_w^{\ 2}}{(T_g^* - T_c^*)^2}} \tag{5}$$

The corresponding relative uncertainty can be calculated by

$$\frac{d\theta}{\theta} = \sqrt{\frac{(T_w - T_c^*)^2 dT_g^{*2}}{(T_g^* - T_c^*)^2 (T_g^* - T_w^*)^2} + \frac{dT_c^{*2}}{(T_g^* - T_c^*)^2} + \frac{dT_w^{\ 2}}{(T_g^* - T_w^*)^2}} \tag{6}$$

The operating temperature of the mainstream thermocouple and the coolant are 1073K and 450~600K respectively. Referring to the temperature measurement value of the

thermocouple, the uncertainty of temperature measured by the thermocouple can be obtained as follows:

$$\frac{dT_g^*}{T_g^*} \le 0.2\%, \quad \frac{dT_w^*}{T_w^*} \le 0.4\%, \quad \frac{dT_c^*}{T_c^*} \le 0.4\% \tag{7}$$

Thus, the maximum uncertainty is:

$$\left(\frac{d\theta}{\theta}\right)_{\max} = 0.6\% \tag{8}$$

3. RESULTS AND DISCUSSION

3.1 Effect of Mass Flow Ratio on OCE

Figures 5-7 shows the effect of K_G on the distributions of the OCE on the vane pressure side and the suction side, for three different temperature ratios equal to 1.5, 1.9 and 2.3, respectively. During the experiments, the gas temperature was maintained constant and equal to 1073 K, and the desired temperature ratio was obtained by changing the coolant temperature. Reynolds number, at the cascade outlet, was also kept constant (Re_g=1.13×10^6). The coordinate original point was considered to be located at the stagnation point. *S* was defined as the whole arc length from the stagnation point to the trailing edge point in the middle cross profile of the vane. *X* represents the coordinate of the arc length, which starts from the stagnation point. The positive and negative direction represent the pressure side and the suction side, respectively. The vertical ordinate θ is defined as the OCE for examining the cooling performance.

It can be seen clearly that the distribution trends of the OCE are similar for the different values of K_T and K_G. The stagnation temperature of the gas was relatively high due to the isentropic stagnation flow. The initial thin boundary layer of the gas also led to the excellent heat convection the external surface of the vane. This means that the heat transfer on the outside seems very remarkable. Therefore, a row of internal impingement holes was arranged to prevent the increase of the wall temperature. The surface temperature decreased considerably in the region of X/S=0~0.4 due to three rows of impingement holes arranged in the internal wall. The heat convection coefficients between the gas and the vane surface were remarkably reduced by the thickened boundary layer. Therefore, the OCE was significantly improved. In contrast, the OCE decreased gradually starting from the point of X/S=0.4 due to the weakened impingement cooling.

The continuous region of X/S= 0.1-0.6, whose OCE was 15% higher than the averaged values of the OCE, was defined as the high efficiency cooling zone. For example, for K_T =1.9 and K_G =0.042, the averaged OCE for high efficiency cooling zone was calculated by 6 thermocouples in the region of X/S= 0.1-0.6, which is 26.2% higher than that of the whole vane.

The large velocity magnitude of the gas led to a relatively high heat transfer coefficient on the suction side. As the outlets of the impingement holes, arranged at the leading edge, slightly deflect to the pressure side, the most of the coolant, ejected from the impingement holes, flow to the trailing edge through the gap of double wall of the pressure side. Although there are more rows of the impingement holes on the suction side than those on the pressure side, the averaged value of the OCE is still lower than that of the pressure side. In addition, there is a pressure gradient in the cascade channel from the pressure side to the suction side, which leads to the lateral movement of the gas. The OCE curves fluctuate evidently in the region of X/S=-0.1~-0.5, because the angles of the impingement holes are

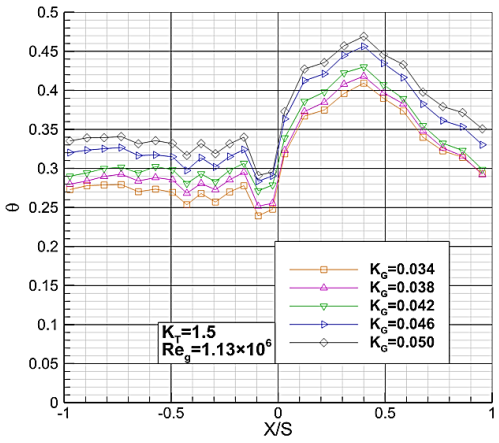

Fig. 5. Effect of K_G on the OCE at K_T=1.5.

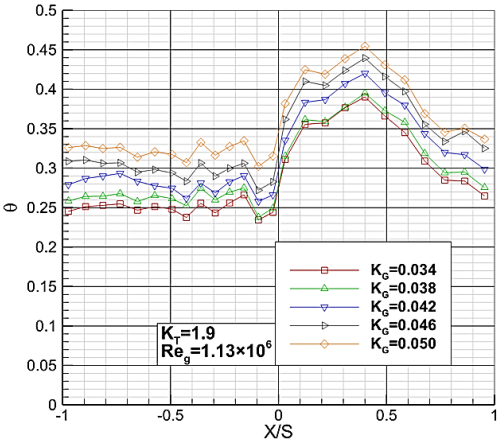

Fig. 6. Effect of K_G on the OCE at K_T=1.9.

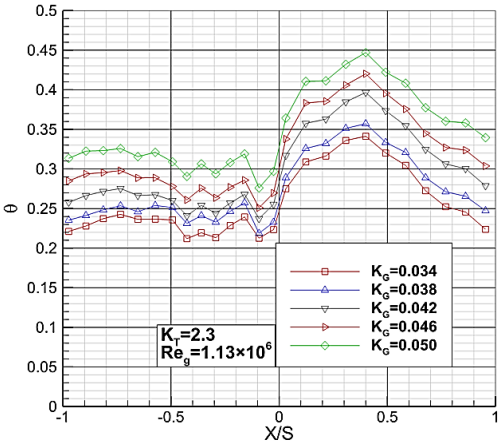

Fig. 7. Effect of K_G on the OCE at K_T =2.3.

perpendicular to the wall. There is no impingement hole in the region of X/S=-0.5~-1, so the OCE changes gently along the middle cross profile of the vane. Although the cutback structure is applied to enhance the internal heat transfer, the OCE is not significantly improved in the cutback region of X/S=-0.9~-1. This may be due to the large heating load and the decreased cooling capacity of the coolant.

Sagot *et al.* (2008) pointed out that the distance between the nozzle and the target plate had little effect on the average Nusselt number through investigation of jet impinging on a plate at a constant wall temperature. It is observed that the turbulence intensity at short distance from the nozzle outlet has little dependence on the distance between the nozzle and the target plate and the jet Reynolds number. The distance between the impingement hole and the wall of the current study falls within the short distance.

The average Nusselt number increases with the increase of jet Reynolds number and cross-flow Reynolds number, and the Nusselt number of pressure surface is more affected by cross-flow than suction surface. The Nusselt number in the area near the stagnation point of the target surface and behind the target surface also increases with the increase of cross-flow. The reason is that under the mixed effect of cross-flow and impinging jet, the horseshoe vortexes in front of the impact point enhance the stretching vortex formed by impinging jet. The superposition effect of the two vortices further enhances the heat transfer on the impact target surface.

When K_G increases from 0.034 to 0.050, the averaged values of the OCE increase by 19.45%, 24.22%, 35.57% respectively for the cases of K_T equal to1.7, 1.9 and 2.3. The averaged OCE for high efficiency cooling zone increased by 15.49%, 17.76%, 31.36%, respectively. An increase of K_G in the gap of the double wall results in the increasing velocity magnitude of the coolant flowing to the trailing edge, thereby enhancing the heat convection of the internal wall. Under different values of K_T, it is obvious that K_G has a weak influence on the distributions of the OCE. This indicates that the cooling mode of the blade will not be changed with the increase of the cooling gas flow. Although an increase of the flow ratio can strongly enhance the comprehensive cooling efficiency, the excessive cooling gas results in the reduction of the work efficiency. Furthermore, it will also bring a large aerodynamic loss. For the engine designing, the flow ratio is a variable factor, which needs to be considered and discussed comprehensively, rather than just for the cooling performance.

3.2 Effect of Temperature Ratio on OCE

Figures 8-10 show the effect of K_T on the curves of the OCE at K_G =0.034, 0.042 and 0.050, respectively. An increase of K_T leads to the decrease of the OCE. The averaged values of the OCE decrease by 16.59%, 9.85% and 5.96%, respectively, at the mass flow ratios of 0.034, 0.042 and 0.050 when K_T changes from 1.5 to 2.3. The averaged OCE for high efficiency cooling zone decreases by 14.20%, 7.55% and 4.82%, respectively. As stated above, K_T has weak influence on the OCE, which is consistent with the conclusion drawn by Venkatasubramanya *et al.* (2012).

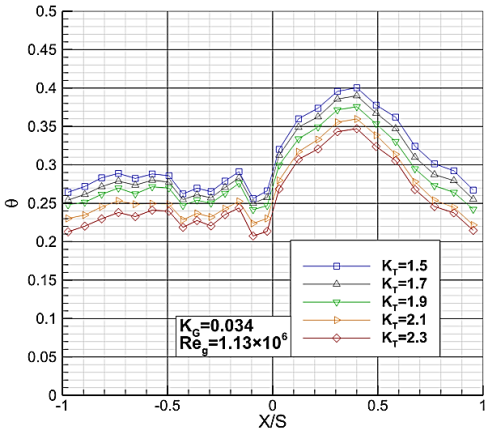

Fig. 8. Effect of K_T on the OCE at K_G =0.034.

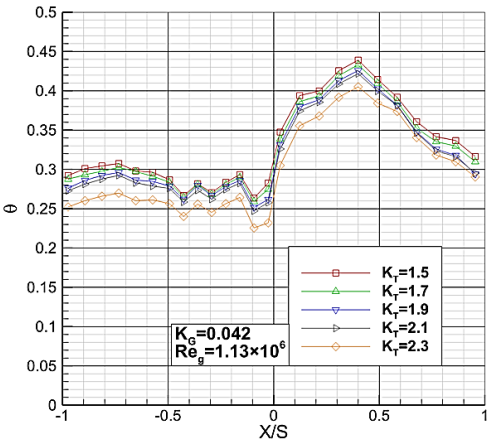

Fig. 9. Effect of K_T on the OCE at K_G =0.042.

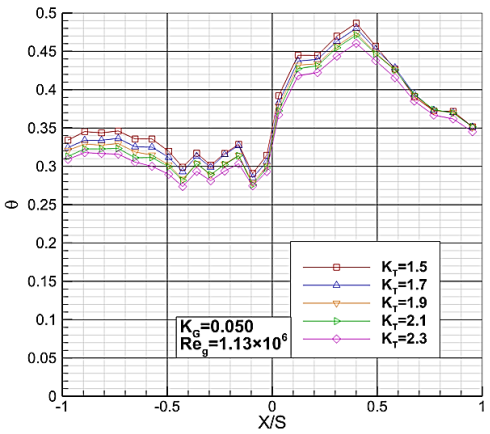

Fig. 10. Effect of K_T on the OCE at K_G=0.050.

According to Eq. (2), the relationship between OCE, the heat transfer coefficient, and the thermal conductivity coefficient can be given as follow:

$$\theta = \frac{1/h_g}{1/h_g + d/\lambda_w + 1/h_c}, \tag{9}$$

where h_g and h_c are the convective heat transfer coefficients of the gas and the coolant respectively, where d is the thickness of the vane wall, λ_w is the thermal conductivity.

The heat convection coefficient is usually converted into a dimensionless Nusselt number Nu_c, which can be described as:

$$Nu_c = \frac{h_c l}{\lambda_c} \quad . \tag{10}$$

The relationship between the Nusselt number and Reynolds number is as follows:

$$Nu_c = C\,\mathrm{Re}_c^{0.8}\ \mathrm{Pr}_c^n \tag{11}$$

where C and n are constants.

As already represented in equation (4),

$$\mathrm{Re} = \frac{\rho_c u l}{\mu} \quad . \tag{12}$$

Combined Eqs. (9)-(11), a new expression of the convective heat transfer coefficient can be defined by the following equation:

$$h_c = C\frac{(\rho_c u)^{0.8}}{l^{0.2}}(\frac{\lambda_c}{\mu})^{0.8}\lambda_c^{0.2}\,\mathrm{Pr}_c^n \quad . \tag{13}$$

The viscosity and thermal conductivity coefficient of the gas have the following relationship with the temperature:

$$\frac{\mu}{\mu_c} = (\frac{T}{T_c})^{0.666}\ , \tag{14}$$

$$\frac{\lambda}{\lambda_c} = (\frac{T}{T_c})^{0.81}, \tag{15}$$

$$\frac{\lambda}{\mu} = (\frac{T}{T_c})^{0.81-0.666} = (\frac{T}{T_c})^{0.144}. \tag{16}$$

Thus, Eq. (12) can be rewritten as follow:

$$h_c = C\frac{(\rho_c u)^{0.8}}{l^{0.2}}(\frac{T}{T_c})^{0.8}\lambda^{0.2}\,\mathrm{Pr}_c^n \ . \tag{17}$$

It can be seen from Eq. (17) that both the thermal conductivity and the convective heat transfer coefficient of the coolant decrease due to the reduction of the temperature; thus, the heat convection performance between the coolant and the wall will be reduced. Meanwhile, the decline of the wall temperature also leads to the decrease of the wall thermal conductivity. Hence, the thermal conductivity of coolant near the internal wall is also weakened. According to Eq. (9), it can be concluded that the OCE decreases after the coolant temperature is reduced. In addition, the decreased temperature of the coolant leads to an increased density. Under the same K_G, the velocity magnitude of the coolant ejected from the impingement hole slows down, which further weakens the heat convection between the coolant and the wall.

3.3 Analysis of Averaged OCE

Figure 11 shows the averaged values of the OCE versus K_T at the different Kw_G values. The averaged value is achieved by 25 thermocouples on the middle cross profile of the vane. It is illustrated clearly that the averaged values of the OCE decrease considerably with an increase of K_T.

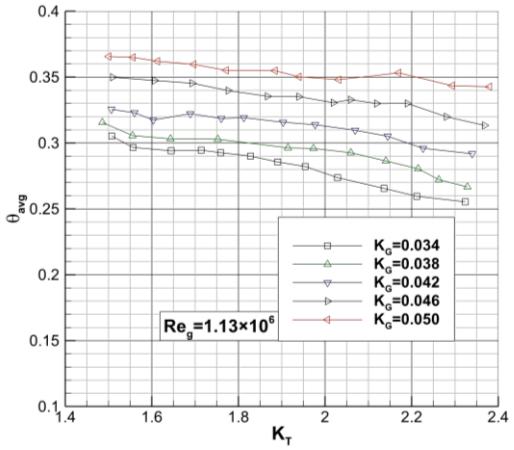

Fig. 11. Effect of K_T on averaged OCE.

Figure 12 shows the averaged values of the OCE versus K_G at different K_T. The OCE presents the different upward trends with an increase of K_G for different values of K_T. The higher K_T leads to a greater influence of K_G, which is illustrated clearly by the compared results of the OCE. The reasonable explanation is that an increased K_T implies in the decrease of the temperature and the increase of the density of the coolant. The small mass flow rate leads to the low speed of coolant. Therefore, the coolant ejected from the impingement hole cannot impinge the wall due to the lack of momentum, thus causing the reduction of the OCE.

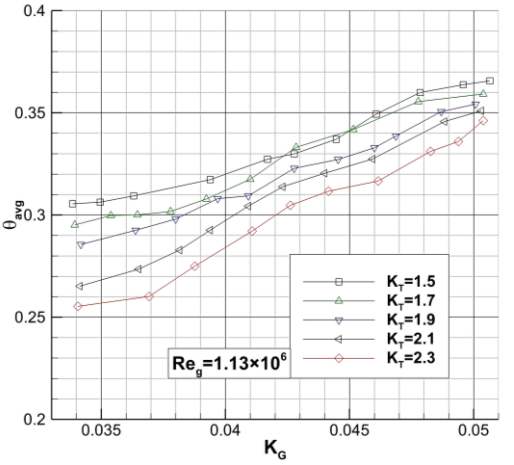

Fig. 12. Effect of K_G on averaged OCE

4. CONCLUSIONS

Both density ratio and dynamic viscosity coefficient ratio are experimentally simulated to achieve more valuable and reliable data in the test of the OCE of the vane. The influences of K_G and the K_T on the OCE are analyzed and discussed. The following conclusions are obtained:

(1) The impingement-cutback structure can significantly enhance the cooling performance of the pressure side of the vane, caused by the cross-flow, from the impingement holes. The lowered flow velocity of the gas, on the pressure side, strengthens the convective heat transfer coefficient. The averaged OCE for high efficiency cooling zone is about 20%~30% higher than that of the whole vane. The OCE of the suction side is relatively stable.

(2) When K_G is increased from 0.034 to 0.050, the averaged OCE of the vane is enhanced by 19.45%, 24.22%, 35.57%, respectively at the temperature ratios of K_T =1.7, 1.9 and 2.3. The increased mass flow rate in the gap of the double wall enlarges the velocity magnitude of the coolant flowing to the trailing edge, thereby enhancing the convective heat transfer on the internal wall. The averaged OCE for high efficiency cooling zone is improved by 15.49%, 17.76%, 31.36%, respectively.

(3) An increase of K_T results in the decrease of the heat convection on the internal wall, thereby leading to a decrease of the OCE. When K_T is increased from 1.5 to 2.3, the averaged OCE is decreased by 16.59%, 9.85% and 5.96% respectively at the corresponding mass flow ratios of 0.034, 0.042 and 0.050. The averaged OCE for the high efficiency cooling zone is weakened by 14.20%, 7.55% and 4.82%, respectively.

(4) K_G and K_T have a weak influence on the distribution trend of the OCE along the middle cross profile. Under the small K_G, the OCE is greatly affected by K_T.

The OCE on the middle cross profile of the vane is developed through this study. The results can provide a valuable data for the optimization and design of the vane cooling structure. The operating conditions, such as the temperature and the pressure, are expected as close to the real operating conditions.

This work can be further developed. Here below, some of the ideas are presented. In future experiments, the influence of higher temperature and centrifugal force load on turbine blades should be considered.

ACKNOWLEDGEMENTS

The authors would like to acknowledge that this study was possible with the support of the National Science Foundation of China (51306126).

REFERENCES

Andrew, C. C. and R. H. David, P. T. Gillespie and R. K. Ireland (2017). Enhancement of impingement cooling in a high cross flow channel using shaped impingement cooling holes. *Journal of Turbomachinery* 132(2), 021001(1-8).

Andrews, G. E. and F. Bazdidi-Tehrani, C. I. Hussain and J. P. Pearson (1989). Small diameter film cooling hole heat transfer: The influence of the number of holes. *ASME 1989 International Gas Turbine and Aeroengine Congress and Exposition*, Toronto, Ontario, Canada.

Boyce, M. P. (2011). *Gas Turbine Engineering Handbook*. Butterworth-Heinemann, Oxford, UK.

Bryant, C. E., C. J. Wiese, J. L. Rutledge and M. D. Polanka (2019). Experimental evaluations of the relative contributions to overall effectiveness in turbine blade leading edge cooling. *Journal of Turbomachinery* 141(4), 041007(1–15).

Ekkad, S. and J. C. Han (2015). A review of hole geometry and coolant density effect on film cooling. *Proceedings of the ASME 2013 Heat Transfer Summer Conference*, Minneapolis, MN, USA

Facchini, B. and L. Tarchi, L. Toni and A. Ceccherini (2010). Adiabatic and overall effectiveness measurements of an effusion cooling array for turbine endwall application. *Journal of Turbomachinery* 132(4), 041008(1–11).

Fechter, S. A. Terzis, P. Ott, B. Weigand, J. V. Wolfersdorf and M. Cochet (2013). Experimental and numerical investigation of narrow impingement cooling channels. *International Journal of Heat and Mass Transfer* 67(Dec), 1208–1219.

Han, J. C., S. Dutta and S. Ekkad (2012). *Gas turbine heat transfer and cooling technology*. Taylor & Francis Group, New York.

Han, J. C., Y. M. Zhang and C. P. Lee (1991). Influence of surface heat flux ratio on heat transfer augmentation in square channels with parallel, crossed and v-shaped angled ribs. *ASME 1991 International Gas Turbine and Aeroengine Congress and Exposition*, Orlando, Florida, USA.

Huang, Y., S. V. Ekkad and J. C. Han (1998). Detailed heat transfer distributions under an array of orthogonal impinging jets. *International Journal of Thermophysics and Heat Transfer* 12(1), 73–79.

Lee, J., Z. Ren, P. Ligrani, M. D. Fox and H. K. Moon (2015). Crossflows from jet array impingement cooling: Hole spacing, target plate distance, Reynolds number effects. *International Journal of Thermal Sciences* 88(Feb), 7–18.

Li, G. C., P. Yang, W. Zhang, Z. Wu and Z. H. Kou (2019). Enhanced film cooling performance of a row of cylindrical holes embedded in the saw tooth slot. *Journal of Heat Mass Transfer* 132(Apr), 1137–1151.

Liu, L., X. Zhu, H. Liu and Z. Du (2018a). Effect of tangential jet impingement on blade leading edge impingement heat transfer. *Journal of Heat and Mass Transfer* 127(Nov), 639–650.

Liu, C. L., G. Xie, R. Wang and L. Ye (2018b). Study on Analogy Principle of Overall Cooling Effectiveness for Composite Cooling Structures

with Impingement and Effusion. *Applied Thermal Engineering* 130(5), 1380–1390.

Lo, Y. H. and Y. H. Liu (2018). Heat transfer of impinging jet arrays onto half-smooth, half-rough target surfaces. *Applied Thermal Engineering* 128(5), 79–91.

Luque, S., T. V. Jones and T. Povey (2017a). Effects of coolant density, specific heat capacity, and biot number on turbine vane cooling effectiveness. *Journal of. Turbomachinery* 139(11), 111005(1-11).

Luque, S. and T. V. Jones (2017b). Scaling of turbine metal temperatures in cooled compressible flows-experimental demonstration of a new theory. *Journal of. Turbomachinery* 139(8), 081001(1-10).

Luque, S., T. V. Jones and T. Povey (2016). Theory for the scaling of metal temperatures in cooled compressible *flows. International Journal of Heat and Mass Transfer* 102(Nov), 331–340.

Mensch, A. and A. T. Karen (2014). Overall effectiveness of a blade endwall With jet impingement and film cooling. *Journal of Engineering for Gas Turbines and Power* 163(3), 031901(1-10).

Mensch, A. and A. T. Karen (2016). Overall Effectiveness and Flowfield Measurements for an Endwall With Nonaxisymmetric Contouring. *Journal of Engineering for Gas Turbines and Power* 128(3), 031007(1-10).

Moussa, A. B., H. Ksibi, C. Tenaud and M. Baccar (2005). Parametric study on the nozzle geometry to control the supercritical fluid expansion. *International Journal of Thermal Sciences* 44(Aug), 774–786.

Murata, A. S., Nishada, H. Saito, K. Iwamoto, Y. Okita and C. Nakamata (2012). Effects of Surface Geometry on Film Cooling Performance at Airfoil Trailing Edge. *Journal of Turbomachinery* 134(5), 051033(1-8).

Qu, L. H., J. Z. Zhang and X. M. Tan (2017). Improvement on film cooling effectiveness by a combined slot-effusion scheme. *Applied Thermal Engineering* 126(5), 379–392.

Rhee, D. H., Y. S. Kang, B. J. Cha and S. Lee (2017). Overall cooling effectiveness measurements on pressure side surface of the nozzle guide vane with optimized film cooling hole arrangements. *ASME Turbo Expo 2017: Turbomachinery Technical Conference and Exposition*, Charlotte, North Carolina, USA.

Sagot, B., G. Antonini, A. Christgen and F. Buron (2008). Jet impingement heat transfer on a flat plate at a constant wall temperature. *International Journal of Thermal Sciences* 47(Oct), 1601–1619.

Schroeder, R. P. and K. A. Thole (2017). Thermal field measurements for a shaped hole at low and high freestream turbulence intensity. *Journal of Turbomachinery* 139(2), 021012(1-9).

Sun, X., G. Zhao, P. Jiang, W. Peng and J. Wang (2018). Influence of hole geometry on film cooling effectiveness for a constant exit flow area. *Applied Thermal Engineering* 130(5), 1404–1415.

Venkatasubramanya, S., S. A. Vasudev and S. Chandel (2012). Experimental Evaluation of Cooling Effectiveness of High Pressure Turbine Nozzle Guide Vane. *ASME 2012 Gas Turbine India Conference*, Mumbai, Maharashtra, India.

Yang, X., Z. Liu, Q. Zhao, Z. Liu, Z. Feng, F. Guo, L. Ding and T. W. Simon (2019). Experimental and numerical investigations of overall cooling effectiveness on a vane endwall with jet impingement and film cooling. *Applied Thermal Engineering* 148(5), 1148–1163.